Microwave Detection of Cracks in Buried Pipes using the Complex Frequency Technique

Fadi Deek and Magda El-Shenawee

Department of Electrical Engineering
University of Arkansas, Fayetteville, AR 72701, USA
eldeek_fadi@yahoo.com, magda@uark.edu

***Abstract*—** This work outlines a new technique for detecting cracks in buried pipes using scattered fields. The matrix pencil method (MPM) is applied on synthetic data to extract the natural frequency poles. A 50 cm long hollow pipe, 2.5 cm in diameter, and 5 mm in thickness is considered. Cracks of arc lengths of 6 cm and 4 cm with a width of 0.5 mm are introduced into the metallic pipes. It is shown that the MPM has the capability to extract distinctive poles associated with these cracks even when the pipe is hidden behind plywood, buried in sand, or when the synthetic data is corrupted with random noise of 10 dB signal to noise ratio.

***Index Terms*—** Complex frequency, crack, GPR, detect, matrix pencil method.

I. INTRODUCTION

Under the effect of pressure, humidity, and other natural or unnatural causes, cracks develop in pipes. The results of such leaks are hazardous to the environment and cause economical losses. Several crack detection techniques have been developed and each serves a specific application [1-5]. Some techniques use trained dogs that can sniff odors of leaking material even from underground [1]. Hardware based techniques include closed-circuit television techniques [2] where a camera is used to record images from the pipes' walls.

In general, non destructive evaluation techniques, NDE, are preferred since they require no excavation. Common NDE techniques use radiography [3] to assess the condition of pipes. An X-ray tube is used to photograph pipes hidden behind walls. The instruments for this method are bulky and hazardous. Also, ultrasonic waves are used to detect cracks on the surfaces of pipes that are partially inaccessible [4]. Such techniques are still inaccurate when detecting corrosion and wall thinning from the inside of the pipe.

Of the many techniques, ground penetrating radars, GPRs, have shown the most flexibility and portability. Ground penetrating radars use electromagnetic waves in order to remotely characterize the physical properties of a media. By doing so, buried targets can be located. For example, Gamba et al. [5] use neural networks to detect hyperbolic signatures of pipes underground. In addition, the media surrounding the defected pipe can be evaluated. As mentioned in [1], the GPR profile is altered whenever a liquid, such as water, leaks into the surrounding.

The method of moments commercial solver was available at our labs, FEKO [6], and was used in this work to simulate cases where a pipe was immersed in free space, hidden behind plywood, or buried underneath sand. The scattered field was solved in the frequency range 50MHz – 10 GHz in steps of 12.5MHz. The present work is not limited to frequency domain solvers, but other time domain software could have been used.

Many available techniques to extract the poles of the complex frequencies such as ESPRIT, Prony and several other singular value decomposition based methods can be found in [7]. Of the many methods, the matrix pencil method (MPM) has shown effectiveness and simplicity [8]. The total least square matrix pencil method (TLSMPM) is the version used in this work. The TLSMPM has shown better performance than other MPM variations when operated under noisy data [9].

A MATLAB algorithm extracts the complex frequencies from the scattered far fields. These frequencies are associated with the cracks on the pipes. This method was inspired by the work in [10] where Blischak et al. used elliptical antennas

with different sized notches to generate unique radio frequency identifications (RFIDs). Each RFID is composed of a set of complex frequencies. The method used for extracting the complex frequencies is known as the matrix pencil method (MPM) [7].

II. MATRIX PENCIL METHOD

The time domain transient response of a scattering object can be expressed by a sum of exponentially decaying signals [8]

$$x(kT_S) = \sum_{i=1}^{M} R_i z_i^k \quad \text{for } k = 0,1,\ldots\ldots N\text{-}1 , \qquad (1)$$

where x(t) is a vector of size N containing the discrete time points, T_s is the sampling period, $R = A_i e^{-j\varphi_i}$ are the complex residues of the matrix pencil poles composed of the amplitudes A_i's and the phase delays Φ_i's. The poles

$$z_i = e^{s_i T_s} = e^{(-\alpha_i + j\omega_i) T_s} \qquad (2)$$

are composed of damping factors α_i and radial frequencies ω_i. The number of poles to be extracted is defined by the parameter M. The first step in extracting the poles is to build the Hankel matrix X_H as [9]:

$$X_H = \begin{vmatrix} x_1 & x_2 & \cdots & x_{L+1} \\ x_2 & x_3 & \cdots & x_{L+2} \\ \vdots & \vdots & \ddots & \vdots \\ x_{N-L} & x_{N-L+1} & \cdots & x_N \end{vmatrix}_{(N-L)x(L+1)} , \qquad (3)$$

where L is known as the pencil parameter.

The singular value decomposition (SVD) is performed on the matrix as in (4) in order to obtain the eigenvectors and eigenvalues as [9]:

$$U \sum V^H = SVD(X_H) . \qquad (4)$$

The matrices U and V are the left and right unitary matrices, respectively. The matrix U is composed of the eigenvectors of the matrix $X_H X_H^H$ where the *superscript H* denotes the conjugate transpose; whereas, V is composed of the eigenvectors of the matrix $X_H^H X_H$. The diagonal matrix $\sum$ contains the singular values of X_H as in (5) [9]:

$$\Sigma = \begin{vmatrix} \sigma_1 & 0 & \cdots & 0 & 0 \\ 0 & \sigma_2 & \cdots & 0 & 0 \\ \vdots & \vdots & \ddots & \vdots & 0 \\ 0 & 0 & \cdots & \sigma_{N-L} & 0 \end{vmatrix}_{(N-L)xL} . \qquad (5)$$

Only the first M eigenvectors of either U or V are kept. Considering U, as an example, (6) shows the truncated matrix.

$$U = [\hat{u}_1, \hat{u}_2, ..., \hat{u}_M]^T . \qquad (6)$$

The complex-frequency poles are the eigenvalues of (7) [9]:

$$[z][I] = \left[U_1^+\right]\left[U_2\right]_{MxM} , \qquad (7)$$

where z is a vector containing the complex poles and I is the identity matrix, + denotes the Moore-Penrose pseudo inverse $X^+ = [X^H X]^{-1} X^H$ and

$$U_1 = [\hat{u}_1, \hat{u}_2, ..., \hat{u}_{M-1}]^T \qquad (8)$$

$$U_2 = [\hat{u}_2, \hat{u}_2, ..., \hat{u}_M]^T . \qquad (9)$$

Once the poles are calculated, the residues, R_i, in (10) can be found by solving the least square problem:

$$\begin{vmatrix} x_1 \\ x_2 \\ \vdots \\ x_M \end{vmatrix} = \begin{vmatrix} 1 & 1 & \cdots & 1 \\ z_1 & z_2 & \cdots & z_M \\ \vdots & \vdots & \ddots & \vdots \\ z_1^{N-1} & z_2^{N-1} & \cdots & z_M^{N-1} \end{vmatrix} \begin{vmatrix} R_1 \\ R_2 \\ \vdots \\ R_M \end{vmatrix} . \qquad (10)$$

The resulting poles are ordered with respect to the singular value matrix in (5). Thus, σ_1 is the maximum entry and σ_{N-L} is the minimal entry of matrix $\sum$. This, also, means that z_1 corresponds to σ_1 and so on.

There are rules of thumb in the literature to what the best values of the pencil parameter L and

the numbers of poles M are [9]. It is recommended that the pencil parameter L have values between $N/3 \le L \le 3N/2$ where N is the number of data points. As for M, the ceiling value depends on (11) where σ_{max} is the maximum singular value found in matrix $\sum$ [8]:

$$\frac{\sigma_c}{\sigma_{max}} \approx 10^{-p}, \qquad (11)$$

where σ_c is another singular value entry down the matrix and p is the number of significant figures of the collected data. The equation states that the singular value that is p orders lower than the maximum singular value is the last pole that needs to be considered [8]. The rest of the poles having lower singular values are considered as noise.

For perfect electric conductors (PEC) structures, a minimal value of M is sufficient to reconstruct the signal within a high accuracy [11]. The value of L = 50 was fixed throughout the analysis.

III. NUMERICAL METHODOLOGY

A. Free space reference configuration

A perfect electric conductor, PEC, pipe is used. The pipe types used in this work are only metallic which are very common in the fuel transport industry like iron cast and steel pipes. Pipes made of dielectrics require further investigation. The length of the pipe is 50 cm, has a diameter of 2.5 cm and a thickness of 0.5 cm. In practical settings the length of the pipe could be in kilometres. However, as a proof of concept the size is limited to 50 cm or less due to the excessive CPU time required by the solver to sweep over the frequency range. For example, the described configurations required ~4 days on an AMD Opteron 246 having four 2 GHz processors. Parallel implementation could solve this issue. Two crack sizes were considered, one having an arc length of 6 cm and the other having an arc length of 4 cm. Cracks are placed at the center of the pipe as shown in Fig. 1. The pipe is excited using a plane wave source with the electric field $\hat{E}_x$ parallel to the axis of the pipe and perpendicular to the crack as shown in Fig. 1. As known, the polarization plays an important factor in picking up the crack signature. The model is solved in the frequency range 50 MHz – 10 GHz at a frequency step of 12.5 MHz. The observation point is located at (0, 0, 60 cm) above the midpoint of the pipe's surface, which is the origin as shown in Fig. 1.

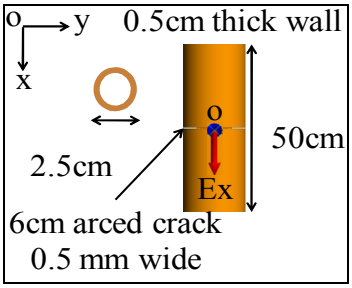

Fig. 1. Pipe configuration and dimensions.

The scattered far field shown in Fig. 2 demonstrates three different cases.

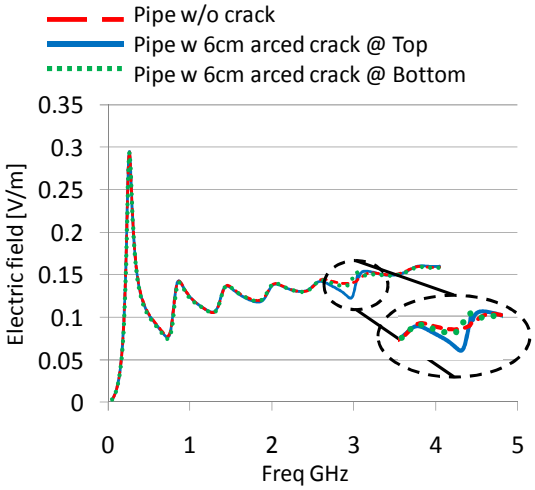

Fig. 2. Scattered fields for pipe in free space.

The dashed line is for a case where a pipe has no cracks. The first resonance of the pipe structure appears as a peak at 260 MHz. The reference resonance of the pipe without a crack stays almost the same when a crack is present due to the miniature size of the crack relative to the pipe. The solid line is the scattered field of the same pipe but with the 6 cm arced crack. The resonance of the pipe appears at 260 MHz and an extra dip appears at 3GHz which is associated with the crack (see the inset). The third case is for the 6 cm arced crack but placed at the bottom side of the pipe, i.e.

on the other side from the illumination source. The dotted line seems to show a small perturbation also at 3 GHz. However, by solely examining the scattered field, no confirmation can be made as to whether a crack exists at the bottom of the pipe or not.

Once the scattered field is collected, a Gaussian filter is applied in order to limit the bandwidth [12] and attenuate residual values of artificial single poles at 0 GHz and 10 GHz. The profile of the filter is shown in Fig. 3.

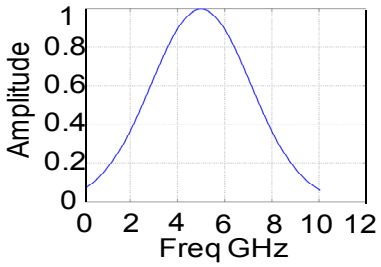

Fig. 3. Gaussian filter profile.

The time domain of the filtered field is obtained using the Fourier transform. The overall time response in Fig. 4a shows a peak at time t=2 ns. This is the time required by the scattered field to propagate from the pipe to the observation point 60 cm away. The matrix pencil method [7-13] is performed on the late time window of the time domain response shown in Fig. 4b. Using the late time response assures removing the illumination effects and makes sure the entire pipe is excited [14].

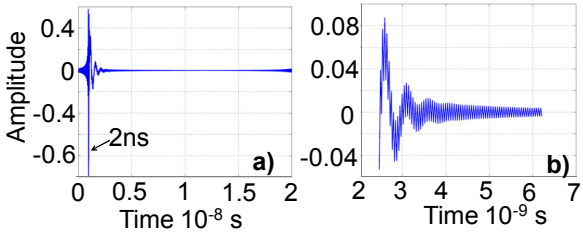

Fig. 4. a) Overall time domain response, b) late time window.

The output of the matrix pencil method is shown in the pole plot of Fig. 5. Only the poles with dominant residues are considered for the three different cases shown in Fig. 2. Consistent with the results of Fig. 2, the resonance of the reference pipe (no cracks) is shown at the pole marked at 260 MHz, which has a dominant residue. The matrix is truncated at M = 4. The pole is indicated by a plus sign in Fig. 5. On the other hand at M = 4, the resonance of the pipe doesn't appear for the case where there was a crack on top or on bottom. Their M was incremented to a value of M = 8 till the main resonance of the reference pipe was extracted. At this value of M, the most dominant pole (largest residue R) appears at a frequency of 2.9 GHz. The 260 MHz reference pole appeared with a significant residue but not the dominant. This signifies the existence of a crack in the pipe. The poles marked with squares and circles in Fig. 5 represent the cases of a crack on the top and on the bottom of the pipe, respectively. Note here that even when a crack was hidden at the bottom of the pipe, a pole associated with the crack appeared as a dominant pole. This was not the case in the far field plot in Fig. 2. This observation confirms that a crack exists in the pipe and shows one of the strengths of the algorithm.

The 4.0 cm arced crack is also introduced at the top of the pipe. A comparison of the scattered field for the pipe is shown in Fig. 6 for the cases with and without the crack. The resonance associated with the crack appears at 6.6 GHz. It was expected that the resonance shifts to a higher frequency compared to the 6.0 cm arced crack since its dimension is smaller.

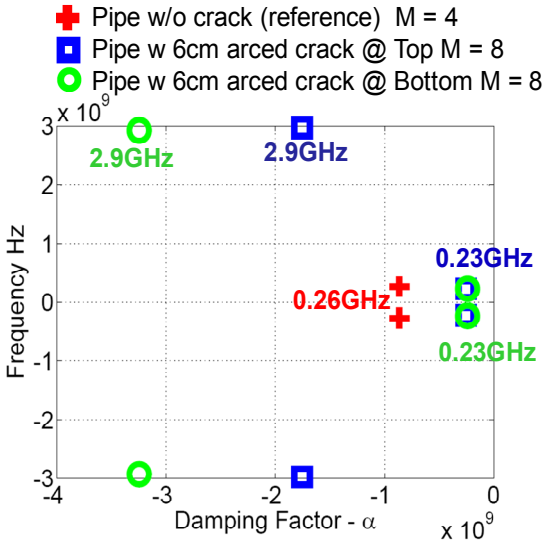

Fig. 5. Pole comparison for reference pipe with no cracks vs. same pipe with 6.0 cm arced crack.

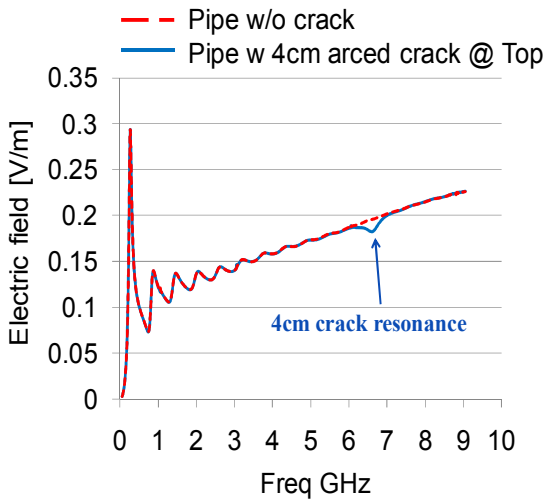

Fig. 6. Scattered field for pipe with a 4.0 cm crack.

The poles of Fig. 6 are plotted in Fig. 7. The algorithm was successful in extracting the reference poles marked as + and the pole associated with a crack marked as a square.

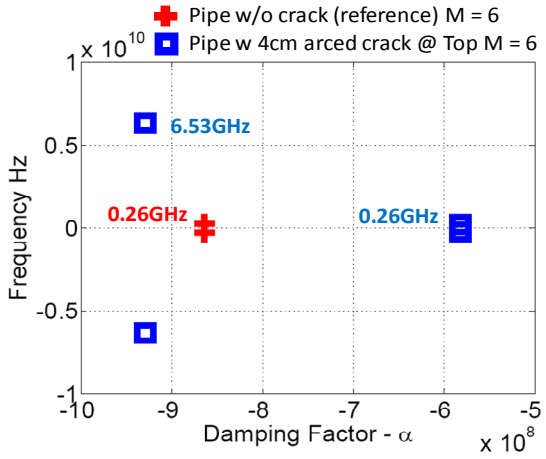

Fig. 7. Pole plot for the reference pipe with and without the 4.0 cm arced crack.

B. Pipe hidden behind plywood

Another case was for a pipe hidden behind a 10.0 cm plywood wall that was infinite in the x-y plane as shown in Fig. 8.

The pipe is located at 5.0 cm away from the wall. Plywood has ε_r = 1.9 and a loss tangent (tanδ) = 0.027. The field is calculated at 60 cm away from the pipe with the origin at the midpoint of the pipe. The illumination was positioned on the opposite side of the pipe.

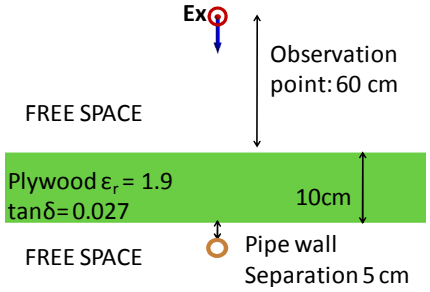

Fig. 8. The configuration of hidden pipe behind plywood wall.

The scattered fields of four scenarios are shown in Fig. 9. The two upper plots of solid and dashed lines represent the pipe in free space without a crack and with a 6.0 cm arced crack, respectively. The bottom two curves are the scattered fields of the hidden pipe with and without the crack. The dotted line is for the pipe with no crack, and the short dashed line is for the same pipe but with the 6.0 cm crack. The magnitude of the scattered field shows attenuation for the hidden case due to the effect of the plywood wall compared with that of free space. However, the scattered fields show that the locations of the resonances are almost the same at 200.0 MHz for the reference pipe and at 3.0 GHz for the hidden pipe with the 6.0 cm crack.

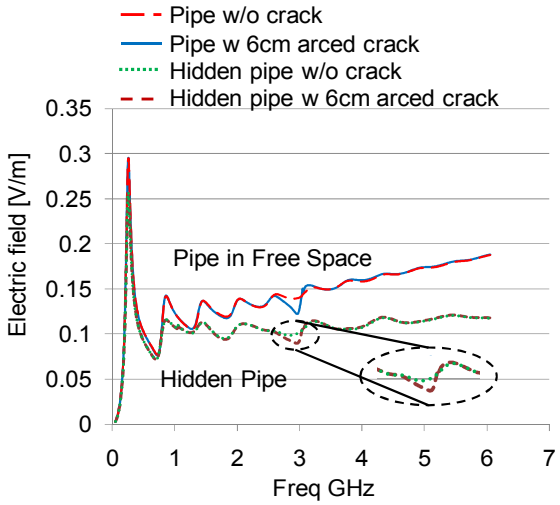

Fig. 9. Comparison of scattered field for pipe in free space vs. pipe hidden behind plywood.

The extracted poles of only the hidden pipe cases are plotted in Fig. 10. Note that the truncation number M is 4 and 10 for the pipe without the crack and with the crack, respectively.

Another common case is for a pipe totally immersed in the plywood wall. The pipe is located at 7.5 cm away from the surface of the plywood interface. The field was computed at the same point as the previous example in Fig. 8. The lower two curves in Fig. 11, where one is dotted and the other is short-dashed, are for an immersed pipe without a crack and a pipe with a crack, respectively. As anticipated, the scattered fields show a shift in the resonance frequency compared with the free space fields due to the contrast between the medium surrounding the pipe in this case.

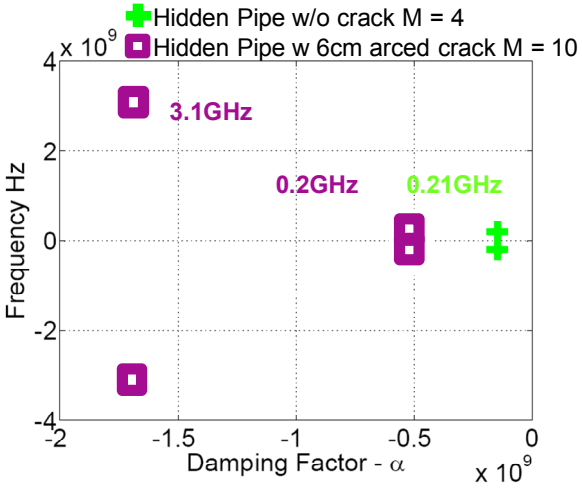

Fig. 10. Pole plot of the hidden pipe with and without the 6cm crack.

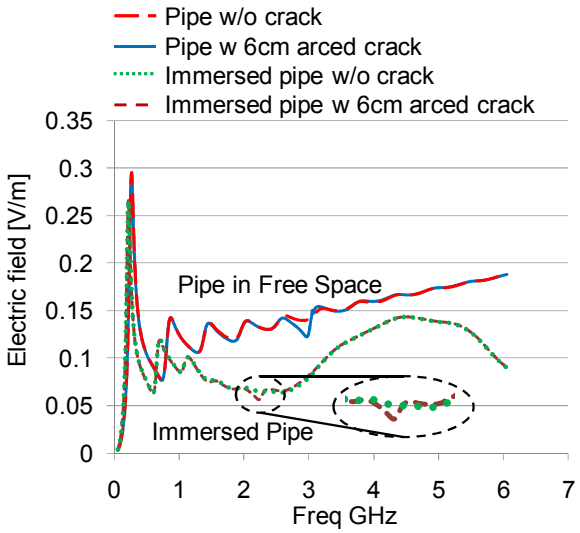

Fig. 11. Comparison of scattered field for the pipe immersed in plywood vs. free space.

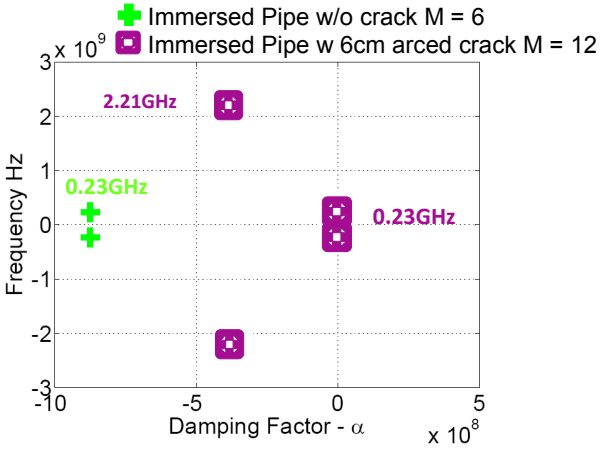

Fig. 12. Pole comparison for immersed pipe cases.

The extracted poles only for the immersed cases are shown in Fig. 12. The reference poles appeared at a frequency of 230 MHz; whereas, the crack pole appeared at a frequency of 2.21 GHz. The pole technique was again successful in detecting the crack in the pipe.

C. Pipe buried underneath sand

A practical case of interest is for a pipe buried underneath sand. The pipe is placed 7.5 cm below the surface of a semi infinite sand plane as shown in Fig. 13. Dry sand has a dielectric constant ε_r = 2.549 and a loss tangent of tanδ = 0.005. Again, the field is calculated at 60 cm away from the pipe with the origin at the midpoint of the pipe as shown in Fig. 1.

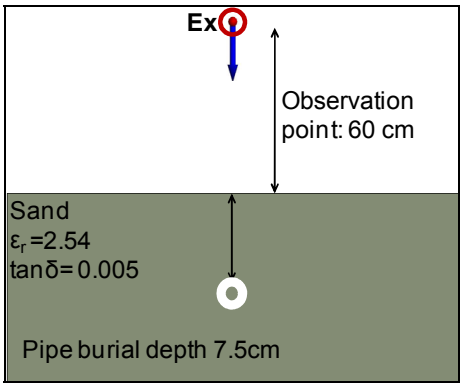

Fig. 13. Configuration of the pipe buried underneath sand.

The four curves in Fig. 14 compare the scattered fields of the buried pipe with that in free space. The lower two curves represent the buried

cases for a pipe without a crack in dotted lines and a pipe with a crack in short dashed lines. The scattered fields show a shift in the position of the resonances due to the medium contrast. The extracted poles show the extra resonance at 1.84 GHz which is associated with the presence of the crack as shown in Fig. 15 marked by a square.

D. Pole extraction using noisy data

The synthetic data obtained using FEKO simulations for the pipe in free space was corrupted with random Gaussian noise with signal to noise ratio SNR = 10dB. The pole plot in Fig. 16 shows that, the pipe with no crack and with the 6 cm crack, the reference poles were extracted at 280 MHz and 220 MHz, respectively.

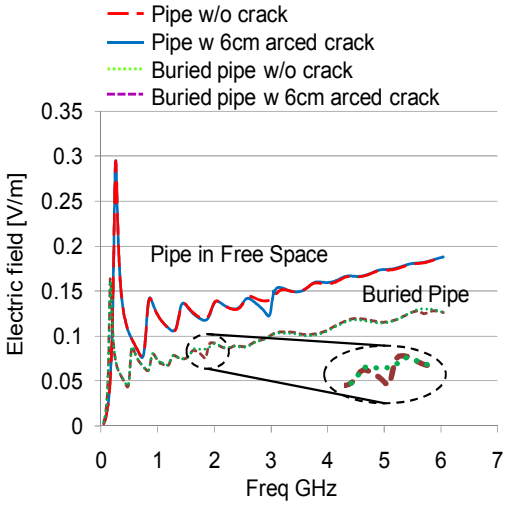

Fig. 14. Comparison of scattered field for pipe in free space vs. pipe immersed in plywood.

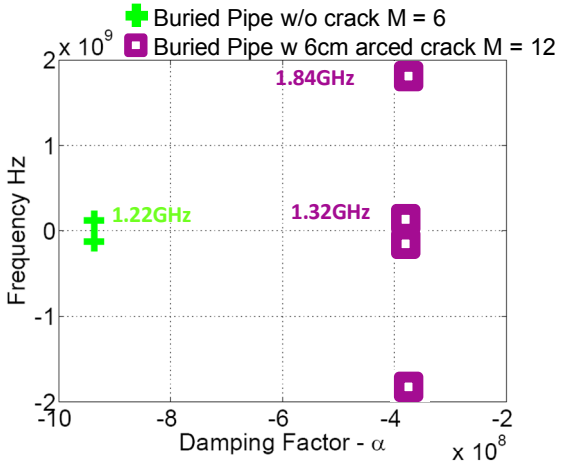

Fig. 15. Pole comparison for immersed pipe cases.

The presence of the noise has caused the reference resonance to shift from 260 MHz for the case of pipe immersed in free space shown in Fig. 2 and in Fig. 5. As well for the case of a pipe with a crack, a dominant pole at 3.24 GHz was extracted as shown in Fig. 16. This shows that the crack detection was successful even with SNR of 10 dB.

As expected, when the SNR is decreased, the pole extraction of the cracks is degraded.

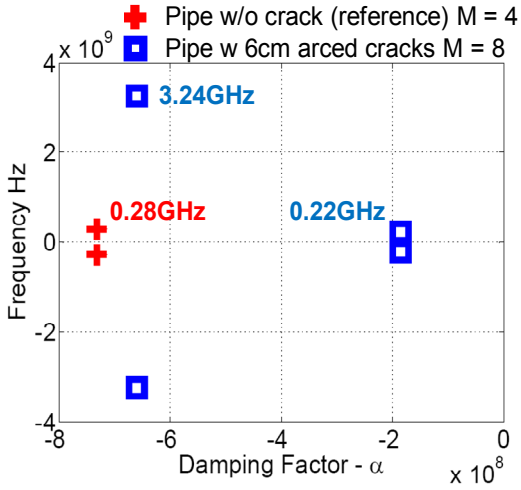

Fig. 16. Poles of the pipe immersed in free space using noisy data of SNR = 10dB.

E. Pole extraction algorithm

The pole extraction algorithm is shown in Fig. 17. Testing the algorithm on buried pipes at larger burial depth with rough interfaces is important for the practical scenario of buried pipes. However, using FEKO, the required CPU time to sweep over the frequency in steps of 12.5MHz was excessive. It is anticipated that the clutter due to the rough surface interface, the attenuation of the soil background, and the larger burial depth of the pipe will affect the sensitivity of the pole extraction. However, the current work has proven the concept of the method in detecting the cracks.

Experiments were conducted inside a custom made $1m^3$ anechoic chamber [15] in order to verify the numerical results. Two Vivaldi antennas, operating between 3 GHz – 10 GHz, were used as transmitters and receivers. The maximum separation distance that can be achieved inside the chamber between the pipe and Vivaldi

antennas was 40 cm. The measured SNR was below -5 dB. The transmitted power was -50 dB [16]. Due to these challenges, the extracted poles were erroneous and resulted in random poles that were at frequencies at least 500 MHz higher than the numerical poles. The experimental work needs a larger chamber to assure far field measurements away from absorbing walls of the small chamber in [16]. Also, a power amplifier is needed to increase the transmitted power. More work will be conducted to validate the algorithm on real data.

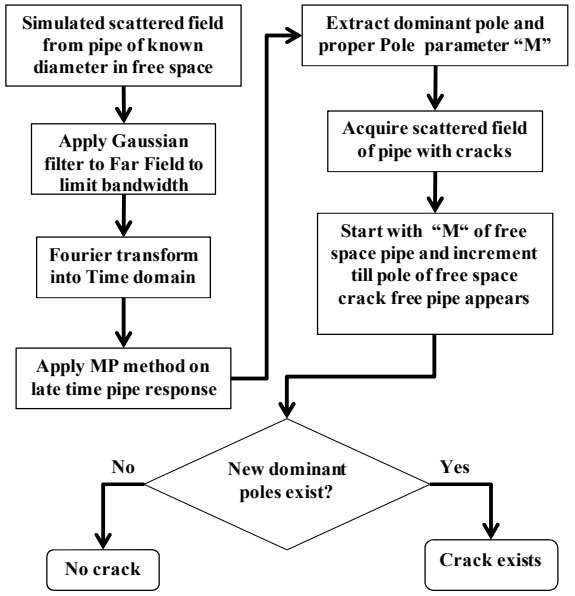

Fig. 17. Pole extraction algorithm.

For a periodically slotted cylinder, the length of the slot is half the wavelength of the resonant frequency [18]. In this work, the length of the crack was observed to be close to half wavelength or multiples as shown in Table 1. Other different lengths of the crack were, also, considered but not included in this work.

Table 1: Crack length versus resonance frequency

Crack lengths (cm)	Resonance frequency (GHz)	Wavelengths of resonance (cm)
6	3.1	9.7
4	6.7	4.5
2	12.7	2.36

IV. CONCLUSION

The numerical algorithm presented here was successful in employing the matrix pencil method for crack detection on the surface of metallic pipes. The algorithm showed success even when noisy data up to SNR of 10 dB was processed for a pipe in free space. However, when the SNR was below 10dB, the extracted poles took random non-resilient values. The susceptibility to noise can be improved by possibly substituting the total least square method by a more noise tolerant approach such as the minimum mean square error [17]. It is possible to integrate the current algorithm with an *inverse scattering algorithm* [15]. This will serve to extract the host's electrical parameters simultaneously with detecting and reconstructing the crack's shape. This is an interesting future research topic.

ACKNOWLEDGMENT

This work was funded by Entergy Incorporation. Special thanks to Electromagnetic Software and Systems Inc. (EMSS USA http://www.emssusa.com) for their technical support and special pricing for FEKO Gold license.

REFERENCES

[1] S. Eyuboglu, H. Mahdi, and H. Al-Shukri, "Detection of water leak using ground penetrating radar," Central Arkansas Water, Little Rock, Arkansas, 2004.

[2] O. Duran, K. Althoefer, and L. D. Seneviratne, "Automated pipe defect detection and categorization using camera/laser-based profiler and artificial neural network," *IEEE Trans. on Automation Science and Engineering,* vol. 4, no. 1, pp. 118-126, January 2007.

[3] Electric Power Research Institute, http://www.epri.com.

[4] M. Silk and K. Bainton, "The propagation in metal tubing of ultrasonic wave modes equivalent to Lamb waves," *Ultrasonics,* vol. 17, no. 1, pp. 11–19, January 1979.

[5] P. Gamba and S. Lossani, "Neural detection of pipe signatures in ground penetrating radar," *IEEE Trans. on Geoscience and Remote Sensing,* vol. 38, no. 2, pp. 790-797, March 2000.

[6] FEKO Field Computations Involving Objects or Arbitrary Shape, http://www.feko.info.

[7] Y. Hua and T. K. Sarkar, "Matrix pencil method for estimating parameters of exponentially damped/undamped sinusoids in noise," *IEEE*

Trans. Acoustic Speech and Signal Processing, vol. 38, no. 5, pp. 814-824, May 1990.

[8] O. M. Pereira-Filho and T. K. Sarkar, "Using the matrix pencil method to estimate the parameters by a sum of complex exponentials," *IEEE Antennas Propagation Magazine*, vol. 37, no. 1, pp. 48–55, February 1995.

[9] Y. Hua and T. K. Sarkar, "Generalized pencil-of-functions method for extracting the poles of an extracting the poles of an electromagnetic system from its transient response," *IEEE Trans. on Antennas Propagation,* vol. 37, no. 2, pp. 229–234, February 1989.

[10] A. T. Blischak and M. Manteghi, "Pole residue techniques for chipless RFID detection," *International Symposium on Antennas and Propagation,* Charleston, SC, pp. 1 - 4, June 2009.

[11] L. Marin and R.W. Latham, "Representation of transient scattered fields in terms of free oscillations of bodies," *Proceedings in IEEE,* vol. 60, no. 5, pp. 640 - 641, May 1972.

[12] R. S. Adve, T. K. Sarkar, O. Maroja, C. Pereira-Filho, and S. M. Rao, "Extrapolation of time-domain responses from three-dimensional conducting objects utilizing the matrix pencil technique," *IEEE Trans. on Antennas and Propagation*, vol. 45, no. 1, pp. 147-156, January 1997.

[13] Y. Hua and T. K. Sarkar, "Matrix pencil and system poles," *Signal Processing,* vol. 21, no. 2, pp. 195-198, October 1990.

[14] J. Chauveau, N. Beaucoudrey, and J. Saillard, "Characterization of perfectly conducting targets in resonance domain with their quality of resonance," *Progress In Electromagnetics Research,* vol. 74, pp. 69–84, 2007.

[15] D. A. Woten, M. R. Hajihashemi, A. M. Hassan, and Magda El-Shenawee, "Experimental microwave validation of level set reconstruction algorithm," *IEEE Trans. on Antennas and Propagation,* vol. 58, no. 1, pp. 230-233, January 2010.

[16] F. Deek, "Microwave detection of cracks in buried pipes using the complex frequency technique," M.S. Thesis, Eleg, U of A, Fayetteville, AR, 2010.

[17] D. Guo, S. Shamai, and S. Verdu, "Estimation of non-Gaussian random variables in Gaussian noise: properties of the MMSE," *International Symposium on Information Theory,* Toronto, Canada, July 6-11, pp. 1083-1087, 2008.

[18] M. Mokhtar, "Analysis of cylindrical frequency selective surfaces," *Proc. of Radio Science Conference,* Helwan, Egypt, pp. B8/1 – B8/8, February 1998.

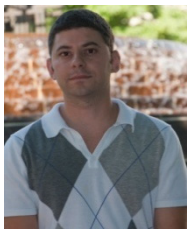

Fadi Deek received his B.S. in Computer and Communications with honors from the American University of Science and Technology, Beirut, Lebanon in 2005. He then worked for three years as an electronic engineer at Fidus Systems. In 2010, he received his M.S. degree in Electrical Engineering from the University of Arkansas, Fayetteville, Arkansas.

Dr. Magda El–Shenawee Dr. El-Shenawee is a Senior member of IEEE since 2002. She received the B.S. and M.S. degrees in electrical engineering from Assiut University, Assiut, Egypt, and the Ph.D. degree in electrical engineering from the University of Nebraska-Lincoln in 1991. In 1992, she worked as a Research Associate in the Center for Electro-Optics at the University of Nebraska where she focused on the problem of enhanced backscatter phenomena. In 1994, she worked as a Research Associate at the National Research Center, Cairo, Egypt, and in 1997, she worked as Visiting Scholar at the University of Illinois at Urbana-Champaign. In 1999, she joined the Multidisciplinary University Research Initiative (MURI) team at Northeastern University, Boston, MA. Dr. El-Shenawee is a member of Eta Kappa Nu electrical engineering honor society.

Currently, Dr. El-Shenawee is a Professor in the Department of Electrical Engineering at the University of Arkansas. Research interests include: biomedical engineering, breast cancer imaging (modeling, detection and treatment), microwave imaging algorithms, anti-personnel mine detection modeling and algorithms, rough surface scattering, subsurface sensing of buried objects, computational electromagnetics, and RF and microwave circuits.